SPE International
Society of Petroleum Engineers

SPE 84086

Will Wireline Formation Tests Replace Well Tests?

T. M. Whittle, SPE, J. Lee, SPE, Baker Atlas; A. C. Gringarten, SPE, Imperial College, UK

This paper was prepared for presentation at the SPE Annual Technical Conference and Exhibition held in Denver, Colorado, U.S.A., 5 – 8 October 2003.

Abstract

Well testing in exploration and appraisal wells has become increasingly unpopular. Reasons include costs, safety and environmental impact. Well testing has also become rare in production wells because of the potential revenue loss during build-ups. Whether suitable alternatives can be found for sampling and reservoir parameter estimation is the subject of regular debate. Alternatives are wireline formation tests in exploration and appraisal, and continuous recording with permanent pressure gauge in production wells.

The quality of pressure and rate transients measured during wireline formation tests has improved greatly in recent years. The transients obey the same laws of physics as those measured during a well test and can theoretically be interpreted in the same way. The scale of the measurements, however, is very different. The challenge is to understand what the wireline formation test interpretation results mean and how they can be upscaled to the information provided by a well test.

The paper discusses these key issues with examples that illustrate the quality of the data and the analysis process. The interpretation methods are essentially the same as those used in well test analysis with the addition of the formation rate analysis plot, which is particularly useful in high permeability formations where other methods are limited by pressure gauge resolution.

Introduction

Well testing is often used in the exploration and development of hydrocarbon reservoirs to:

1. Obtain representative formation fluid samples;
2. Measure initial reservoir pressure;
3. Demonstrate and/or establish well productivity;
4. Determine permeability thickness product, kh, and skin, S;
5. Identify the drainage area of the well and any boundary effects that may exist within;
6. Identify and quantify depletion.

These objectives can be compared with those of a wireline formation test:

1. Determine formation pressures at zones of interest, and establish pressure gradients for fluid type identification;
2. Identify zones in hydraulic communication or isolation;
3. Collect representative formation fluid samples;
4. Estimate formation fluid mobility.

Clearly, an overlap exists between the two techniques and whether one can replace the other depends on the specific well objectives. For example, some exploration wells are drilled solely for the purposes of confirming the existence of a hydrocarbon column, in which case a wireline formation test is probably sufficient. Other wells may be drilled to prove a minimum volume of hydrocarbon-fluids-in-place for which a reservoir limit well test is then the only option. Between these two extremes, there are a number of cases where it may be unclear whether a well test is required.

The strongest reason not to perform the well test is, of course, financial. Environmental cost is also increasingly important. The decision to test has to be made taking into account the cost of acquiring the information. This implies an understanding of what that information is and whether it can be acquired by other means.[1]

The collection of representative fluid samples is often an important objective of both wireline formation tests and well tests. This is clearly an area of overlap where wireline formation tests have proved to be a valid alternative to well tests.[2] However, there are cases where the collection of fluid samples at surface may also be considered necessary.[3]

In this paper, the focus is on the information that can be obtained from the pressure transients recorded during a wireline formation test and how the information compares with the data recorded during a well test.

The interpretation of pressure transients from well tests has been the subject of much research and development over the last thirty years and, with the introduction of fast PCs and properly designed analysis software, the process has become fairly standard. The interpretation of pressure transients from

wireline formation tests is a more recent development and it is noted that:

1. The established methods used in well testing are not always applied to wireline formation testing.
2. In high permeability, there is likely to be insufficient gauge resolution to record an interpretable pressure transient.
3. Well test analysis software has not been adapted for use with wireline formation test data.
4. Analysis is often performed by the service company using proprietary software.

This paper discusses the application and limitations of established methods of analysis used in well testing to the interpretation of pressure transients recorded during wireline formation tests taking into account the differences in scale and geometry. Familiarity with well test interpretation techniques[4] is assumed. Once it is understood how the information obtained from a wireline formation test compares to (or differs from) a well test, it should be easier to judge whether a well test is required. Three field examples are included to illustrate the methods.

Upscaling permeability from the scale of the wireline formation test to that of the well test is fundamental to the estimation of well productivity. Simple methods are described including their inherent limitations.

Wireline Formation Test Analysis

Fig. 1 illustrates the fundamental types of wireline formation test considered in this study.

Single Snorkel. Various authors[5-7] have investigated the theoretical pressure transient response of the single snorkel (probe) type of configuration. The approach in this paper is to consider the withdrawal of a slightly compressible fluid at constant rate from a spherical source with storage and skin in an infinite homogeneous reservoir. The difference between the actual probe-well geometry and the spherical source is approximated by the skin factor. Solutions to the spherical source problem are well documented. The selection of the correct independent dimensionless parameters and the addition of storage and skin are discussed in Appendix A. A type curve representation of the model is shown in Fig. 2.

Drawdown Mobility. Examination of Eq. (A-9) reveals that, for spherical flow, the dimensionless pressure response, *pD,* tends to steady state conditions as time increases and reduces to

$$p_D = 1 + S_p \tag{1}$$

where S_p is the spherical or probe skin. Using customary units as defined in Table 5 and the definition of p_D in Eq. (A-1), Eq. (1) rearranges to

$$\frac{k_{xyz}}{\mu} = 1169\frac{q(1+S_p)}{r_s \Delta p} \tag{2}$$

The following equation[6] is often used to calculate drawdown mobility, k_d/μ, (also in customary units):

$$\frac{k_d}{\mu} = 2338\frac{C' \cdot q}{r_e \Delta p} \tag{3}$$

where C' is a shape factor to account for the presence of the borehole, and r_e is an effective probe radius. The comparison of Eqs. (2) & (3) implies that the actual flow into a probe located at the side of a wellbore is equivalent to a spherical source with the same radius as the probe and a skin, *Sp*, defined by equating Eqs. (2) & (3):

$$S_p = 2C'\frac{r_s}{r_e} - 1 \tag{4}$$

In practice, the rate during a test is varying continuously and consequently Eq. (3) is not strictly valid.

Formation Rate Analysis (FRA). A technique[8] for formation tester pressure data, FRA is based on the material balance equation for the formation tester's flow-line volume with the consideration of pressure and compressibility of the enclosed volume. FRA allows for the variation in flow rate and includes both drawdown and buildup pressure data. It assumes Darcy flow from the reservoir to the probe:

$$p(t) = p^* - \left(\frac{\mu}{k_{FRA} G_0 r_p}\right) q_{sf}(t) \tag{5}$$

The geometric factor, G_0, accounts for the complex flow geometry near the probe. The formation rate at the sandface, $q_{sf}(t)$, relates to the measured piston movement within the tool, dV/dt, as follows:

$$q_{sf}(t) = \left(c_{sys} V_{sys} \frac{dp(t)}{dt} + \frac{dV}{dt}\right) \tag{6}$$

Solving Eqs. (5) & (6) using the entire pressure response (flow and shut-in) results in estimates of initial pressure, p^*, mobility, k_{FRA}/μ, and system compressibility, c_{sys}. A plot of pressure, $p(t)$, versus formation rate, $q_{sf}(t)$ should be linear when the test conforms to Darcy's law and it is therefore a useful quality control check for the test.

Transient Analysis. The constant rate spherical source solution with storage and skin is adapted to a variable rate using superposition.[9] Comparison of its response with the FRA method indicates that a dimensionless geometric skin of approximately 1.8, is required to obtain the same mobility from each method and reflects the fact that FRA takes into account the non-spherical flow geometry due to the presence of the wellbore. Numerical studies that consider the probe geometry and the wellbore have confirmed that the spherical source model matches the numerically modeled transients with errors no greater than 13% when the appropriate skin factor is used.[10]

Field Example 1. The measured pressure and rate response recorded during a wireline formation test is illustrated in Fig. 3. The figure also includes a match of the spherical source model to the data using the input data and match parameters detailed in Table 1. The formation rate analysis (Fig. 4) results in a higher mobility than that derived from the transient analysis (Fig. 5) which also predicts a lower than expected skin. This might be due to permeability anisotropy.[10] FRA

mobility is normally close to spherical mobility, but it is affected by anisotropy. The transient analysis should always predict spherical mobility regardless of anisotropy although the skin will change accordingly.

The radius of investigation, r_i, is calculated using the following approximation (Ref. 9, Eq. 2.41):

$$r_i \approx 1.78\sqrt{\frac{a_2 k_{xyz}\Delta t_{si}}{\phi\mu c_t}} \quad (7)$$

In this example, the calculated value (120 cm) based on the entire shut-in duration (204 s) is probably realistic. However, in higher permeabilities, the limitation in pressure gauge resolution will be reached much earlier after which no meaningful transients are recorded and the radius of investigation is consequently reduced.[11] Then, in the absence of measurable pressure transients, the FRA method becomes the only means to estimate mobility.

To illustrate the impact of high permeability on the pressure transients, analytical simulations of the example test were made using various mobility values but keeping everything else the same. A synthetic pressure gauge resolution of 0.01 psi was applied to the simulated pressures and the resulting derivative response of the buildup pressure transients are shown in Fig. 6. Above 100 mD/cp, the transient response begins to be lost due to the lack of pressure resolution.

Field Example 2: Application to thin beds. This example (see Fig. 7) includes a repeat test (used to validate pressures recorded during the initial test) and demonstrates the high quality and repeatability of data that can be acquired during such tests (Fig. 8 & Fig. 9). The inclusion of upper and lower boundaries to simulate thin beds, which is suggested by the stabilization in the derivative response in Fig. 9, necessitates the introduction of permeability anisotropy into the model as discussed in Appendix A. Table 2 details the input data, match parameters and results. The resultant log-log match is shown in Fig. 10. In this case, the FRA (Fig. 8) and spherical mobilities are very similar which suggests that the formation permeability is isotropic (k_z/k_{xy}=1).

Only one of either the bed thickness or the permeability anisotropy can be evaluated from a single probe type data analysis. Assuming one of these parameters is available from other sources of data (usually the thickness from logs, cores or images), then the other (permeability anisotropy) can be estimated from the analysis.

The radius of investigation calculated in this example (100cm) is less than that in Example 1 even though the permeability is higher. This is because the duration of useful build-up transient is much less.

Dual Snorkel. This problem has also been well documented.[12,13] In this study a simplified approach is taken which appears to yield adequate results. The source probe is considered as a spherical source with storage and skin as described above and in Appendix A. The observation probe measures the pressure at a distance Δz above or below the producing source probe. Appendix A describes the independent dimensionless groups that govern the behaviour of this model and Fig. 11 is a type curve representation of the pressure transient response. To validate the model, the response of the observation probe under different anisotropy conditions was compared to that predicted by Goode and Thambynayagam using the same set of data (Table 3). The comparison plot (Fig. 12) shows a good agreement between the two.

Straddle Packer. The model used to describe the pressure transient response of a wireline formation test using inflatable straddle packers is identical to that for a partially completed well.[14] The dimensionless groups are defined in Appendix B which inlcude the location of an observation probe above or below the straddle packers. In ideal conditions, such a test can quantify horizontal and vertical permeability as illustrated in the next field example.

Field Example 3: Straddle Packer Pumping Test. The pressure and rate history measured while pumping via straddle packers are shown in Fig. 13. Table 4 details the input data and results of the match using the partial completion model as illustrated in Fig. 14 The derivative response shows a negative half slope indicative of spherical flow. However, radial flow has not developed and therefore the estimate of horizontal permeability thickness, $k_{xy}h$, represents a minimum value since any higher value could result in an equally good match. A good field example where radial flow is reached can be found in Hurst, et al.[15]

Because the rates are much higher during pumping with straddle packers, the transient response is much better than that obtained using a probe type pressure test. Compared to a well test, these rates are still quite low and in high permeability, gauge resolution will continue to limit the quality of pressure transients. In open hole, there is also a time limit on how long the straddle packers can remain safely in place. This may reduce the available pressure transient data and could compromise the analysis.

The simulated pressure response that could be measured at an observation probe located 180 cm above the mid-point of the open interval is illustrated in Fig. 15 and its derivative in Fig. 14.

Upscaling

Once a number of formation tests have been conducted on a well in a potential producing interval, the challenge is to upscale the interpreted permeability values of each test to a single permeability thickness of the entire interval with a view to predicting the performance of a potential production well. This process can only be done with information from other sources (e.g. logs, cores and images) for the reasons discussed in this section.

First, it is assumed that the reservoir interval can be described as a sequence of n homogeneous (but possibly anisotropic) layers. Then, the average permeability thickness product of such a multi-layered reservoir can be calculated from the individual layer properties, thus:

$$\overline{kh} = \sum_{i=1}^{i=n} k_{xyi} h_i \quad (8)$$

Assuming that the result of a wireline formation test analysis is a description of spherical permeability, k_{xyz}, for each layer, the additional information required to calculate the average permeability thickness is the permeability anisotropy, k_{zi}/k_{xyi}, and the thickness of each layer, h_i:

$$\overline{kh} = \sum_{i=1}^{i=n} \sqrt{\left(\frac{k_{xy}}{k_z}\right)} k_{xyi} h_i \qquad (9)$$

Permeability anisotropy may result from a wireline formation test analysis, but the thickness of each layer is information that is obtained from other sources (usually logs but, at the smaller scale, images may be useful as well). It must also be assumed that the spherical permeability derived from the formation test analysis relates to a single layer and is not influenced by adjacent layers. Otherwise (for example when the probe is close to a layer boundary), FRA may provide a better esimate of permeability.[10] As well as from cores, permeability anisotropy may be derived from resistivity logs.[16]

Having estimated permeability thickness, the prediction of well productivity can be calculated. For example, the simplest expression for the productivity index assumes pseudo-steady state flow to a fully completed vertical well in a circular drainage area:[17]

$$PI = \frac{q}{\Delta p} = \frac{a_1 \overline{kh}}{B\mu\left(\ln\frac{r_e}{r_w} - 0.75 + S\right)} \qquad (10)$$

Rate refers to standard surface conditions, hence the introduction of the formation volume factor, B. The additional parameters that need to be estimated are drainage radius, r_e, and skin S. The former relies on knowledge of the extent of the reservoir whilst the latter depends on the completion of the well.

Conclusions

- A well test can be replaced by a wireline formation test if the objectives of the well test can be met by the wireline formation test.
- In lower permeability reservoirs (mobilities less than about 100 mD/cp), the quality of data recorded by wireline formation test tools is suitable for pressure transient interpretation. In higher permeability, the resolution of the pressure gauge limits the quality of the data often precluding transient analysis and the FRA method then provides the best estimate of mobility.
- In general, pressure transient analysis of wireline formation tests provides estimates of spherical permeability. In thin beds of known thickness or in cases where an observation gauge is used to measure vertical interference, there is also the possibility to evaluate permeability anisotropy.
- Upscaling the permeabilities derived from wireline formation tests to a prediction of the performance of a fully completed well is possible provided a number of assumptions are made. In particular, the permeability anisotropy must be known or estimated.
- A wireline formation test is a cost effective alternative to a well test for the purposes of obtaining high quality dynamic pressure and flow information albeit at a reduced scale.

Nomenclature

Table 5 defines the symbols, units and conversion factors referred to in the text.

Acknowledgements

The Authors would like to thank Baker Atlas for their kind permission to present this paper. The authors would also like to thank Alberto Mezzatesta, Janusz Buczak and Karen Bush with Baker Atlas for their useful comments and editing help while writing the paper.

References

[1] Frimann-Dahl, C., et al.: "Formation Testers vs DST – The Cost Effective Use of Transient Analysis to Get Reservoir Parameters," paper SPE 48962 presented at the 1998 SPE Annual Technical Conference and Exhibition, New Orleans, Louisiana, Sep. 27-30.

[2] Witt, C. J., et al.: "A Comparison of Wireline and Drillstem Test Fluid Samples from a Deepwater Gas-Condensate Exploration Well," paper SPE 56714 presented at the 1999 SPE Annual Technical Conference and Exhibition, Houston, Texas, Oct. 3-6.

[3] Dybdahl, B. and Hjermstad, H.: "A systematic Approach to Sampling during Well Testing," paper SPE 69427 presented at the 2001 SPE Latin American and Caribbean Petroleum Engineering Conference, Buenos Aires, Argentinan Mar. 25-28.

[4] Bourdet, D.: *Well Test Analysis: The Use of Advanced Interpretation Models,* Elsevier, (2002) **1**.

[5] Moran, J.H. and Finklea E.E.: "Theoretical Analysis of Pressure Phenomena Associated with the Wireline Formation Tester," *JPT* (Aug. 1962) 899-908; *Trans*., AIME, 225.

[6] Dussan, F., and Sharma Y.: "An Analysis of the Pressure Response of a Single-Probe Formation Tester," paper SPE 16801 presented at the 1987 SPE Annual Technical Conference and Exhibition, Dallas, Texas, Sep. 27-30.

[7] Stewart, G., and Whittman, M.: "Interpretation of the Pressure Response of the Repeat Formation Tester." SPE 8362 presented at the 1979 SPE 54th Annual Technical Conference and Exhibition, Las Vegas, Sep. 23-36.

[8] Kasap, E., et al.: "Formation-Rate-Analysis Technique: Combined Drawdown and Buildup Analysis for Wireline Formation Test Data," *SPEREE* (June 1999), 273

[9] Earlougher, R. C.: *Advances in Well Test Analysis, Monograph Series, Society of Petroleum Engineers of AIME, Dallas, (1977)* ***191.***

[10] Theocharis, L.: "Upscaling from Formation Testing to Well Testing," MSc project, Imperial College of Science, Technology and Medcine, London, England (2002) **29**.

[11] Daungkaew, S.: "Frequently Asked Questions in Well Test Analysis" paper SPE 63077 presented at the 2000 SPE Annual Technical Conference and Exhibition, Dallas, Texas, Oct. 1-4.

[12] Goode, P.A. and Thambynayagam, K.M.: "Permeability Determination With a Multiprobe Formation Tester," *SPEFE* (Dec 1992) 297 (SPE 20737)

[13] Proett, M. A., et al.: "Advanced Dual Probe Formation Tester with Transient, Harmonic, and Pulsed Time-Delay Testing Methods

Determines Permeability, Skin, and Anisotropy" SPE 64650 presented at the SPE International Oil and Gas Conference and Exhibition, Beijing, China, 7-10 Nov. 2000.

[14] Theuveny, B.C., et al.: "Pressure Taransient Analysis for Single Well/Reservoir Configurations (Considering Partial Penetration, Mixed Boundary, Wellbore Storage, and Skin Effects," paper SPE 13627 presented at the 1985 SPE California Regional Meeting, Bakersfield, California, Mar. 27-29.

[15] Hurst, S.M., et al.: "Using the Cased-hole Formation Tester Tool for Pressure Transient Analysis," paper SPE 63078 presented at the 2000 SPE Annual Technical Conference and Exhibition, Dallas, Texas, Oct 1-4.

[16] Georgi D., et al.: "On the relationship between Resistivity and Permeability Anisotropy," paper SPE 77715 presented at the 2002 SPE Annual Technical Conference and Exhibition, San Antonio, Texas, Sep. 29-Oct 2.

[17] Matthews, C.S. and Russel, D.G.: *Pressure Buildup and Flow Tests in Wells*, Monograph Series, Society of Petroleum Engineers of AIME, Dallas (1967) 1.

[18] Gringarten, A. C., et al.: "A Comparison of Different Skin and Wellbore Storage Type Curves for Early Time Transient Analysis" SPE 8205 presented at the 1979 SPE 54th Annual Technical Conference and Exhibition, Las Vegas, Sep. 23-36.

[19] Bourdet, D., et al.: "Use of Pressure Derivative in Well-Test Interpretation," *SPEFE* (June 1989) 293-302 (SPE 12777).

[20] Bourdet, D., et al.: "A New Set of Type Curves Simplifies Well Test Analysis," World Oil (May 1983) 95-106.

[21] Kucuk, F.: "Generalised Transient Pressure Solutions with Wellbore Storage," paper SPE 15671, submitted for publication, April 18th 1986.

[22] Stehfest, H.: "Algorithm 368, Numerical Inversion of Laplace Transforms," D-5 Communication of the ACM (Jan. 1970), 13, No. 1 47-49.

[23] Gringarten, A. C., and Ramey, H. J.: paper SPE 3818 "The Use of Source and Green's Functions in Solving Unsteady-Flow Problems in Reservoirs," *SPEJ* (Oct. 1973) 285-296

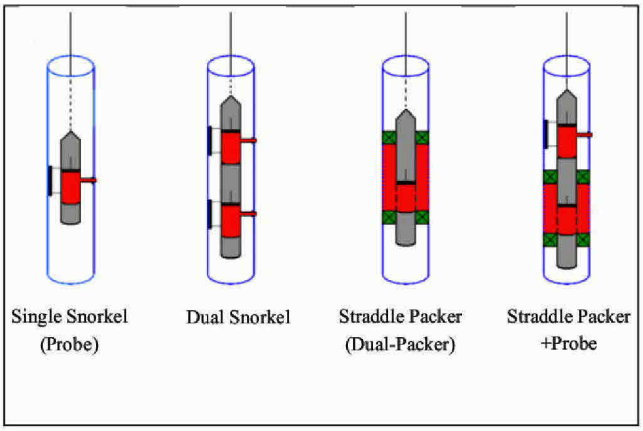

Fig. 1: Schematic of types of wireline formation test

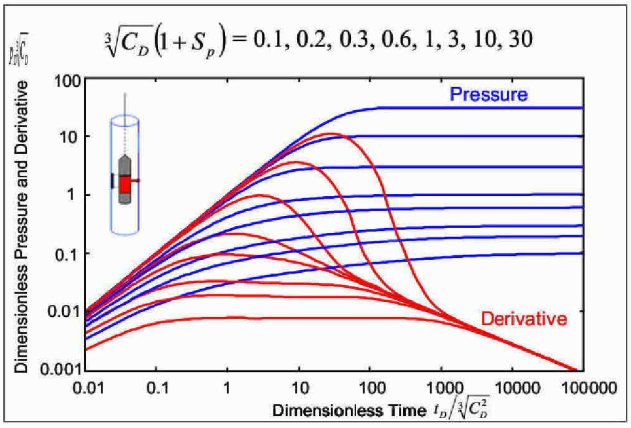

Fig. 2: Type Curve representation of a single snorkel test in an infinite acting homogeneous reservoir with storage and skin

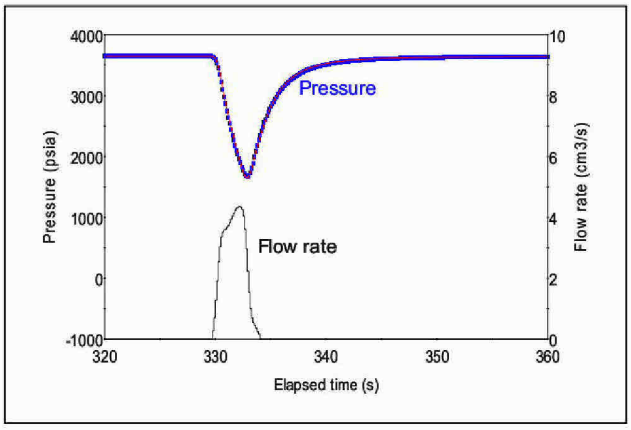

Fig. 3: Example 1. Single snorkel formation test

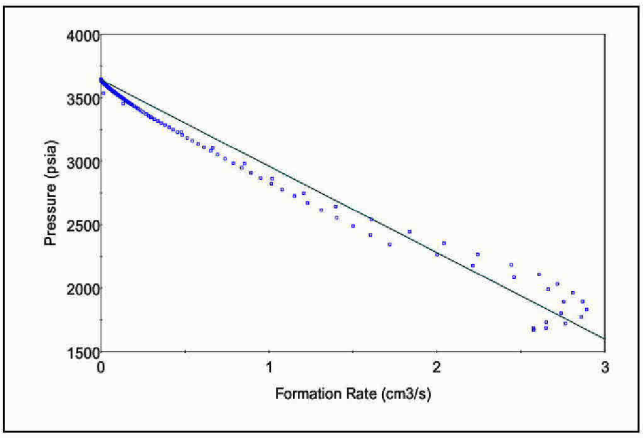

Fig. 4: Example 1. Formation Rate Analysis (FRA)

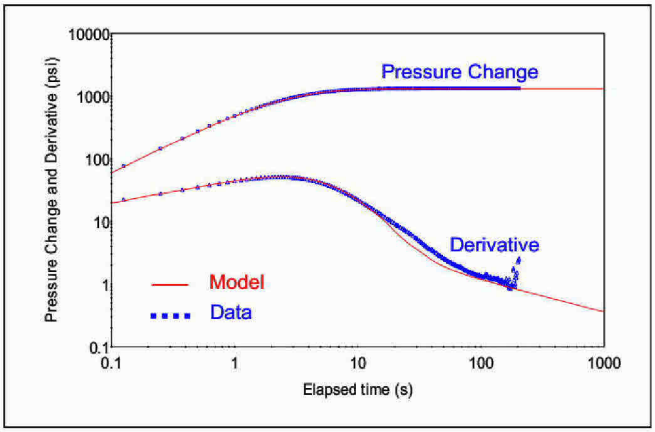

Fig. 5: Example 1. Log-log plot of match to build-up data

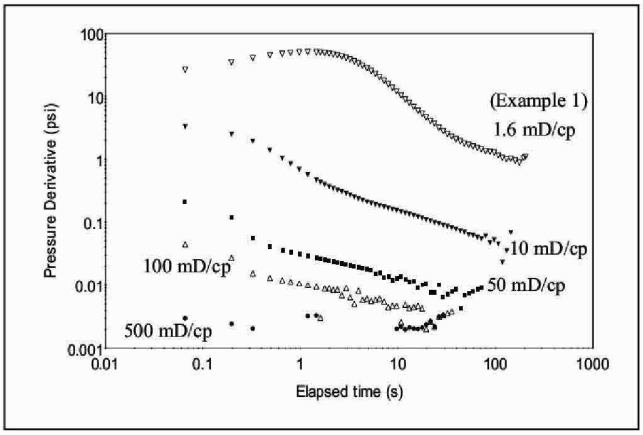

Fig. 6: Simulated pressure derivative response for various mobilities assuming a pressure gauge resolution of 0.01 psi using input data from Example 1

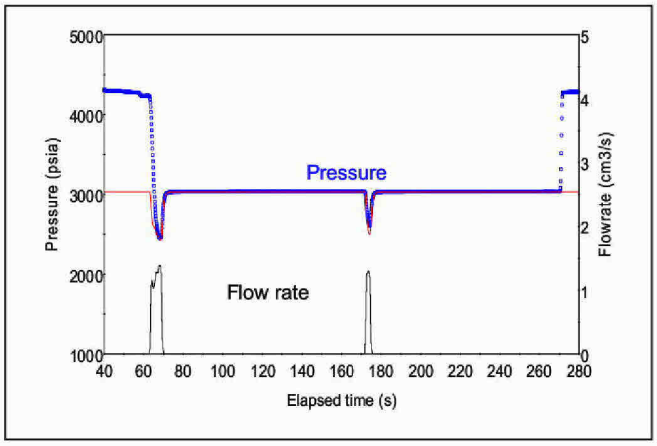

Fig. 7: Example 2. Single snorkel formation test with repeat

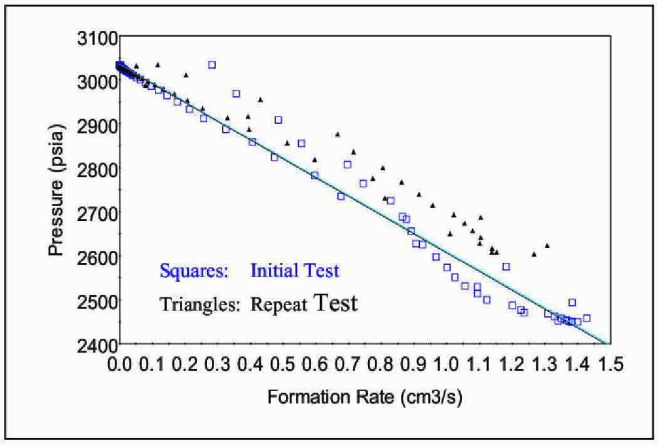

Fig. 8: Example 2. FRA for initial and repeat test

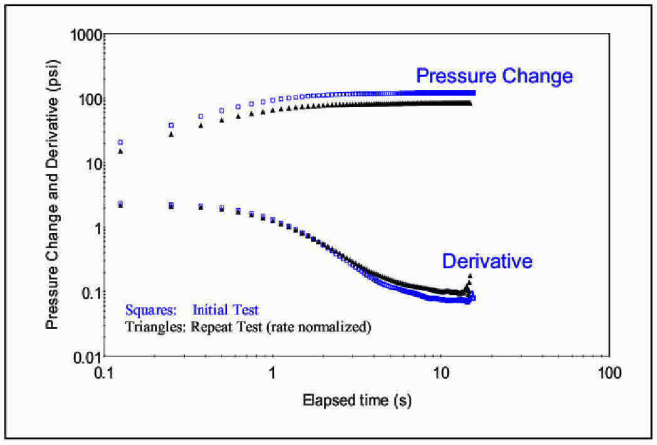

Fig. 9: Example 2. Log-log diagnostic plot of Initial and Repeat Test

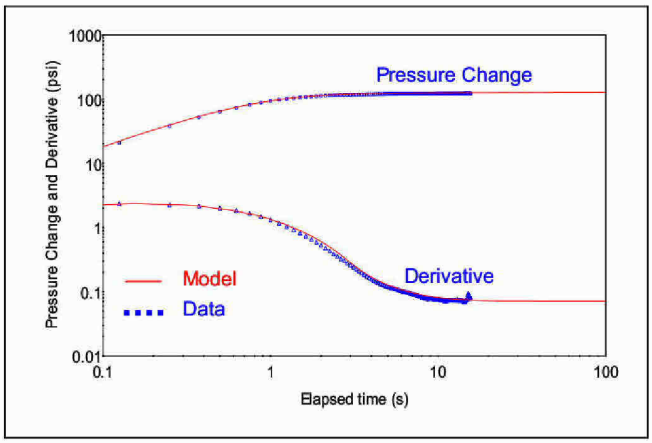

Fig. 10: Example 2. Log-log plot of match to initial build-up data

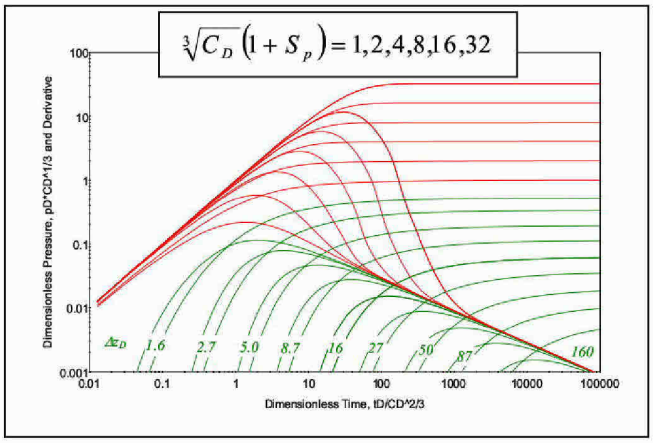

Fig. 11: Type curve representation of a dual snorkel test in an infinite acting homogeneous reservoir with storage and skin

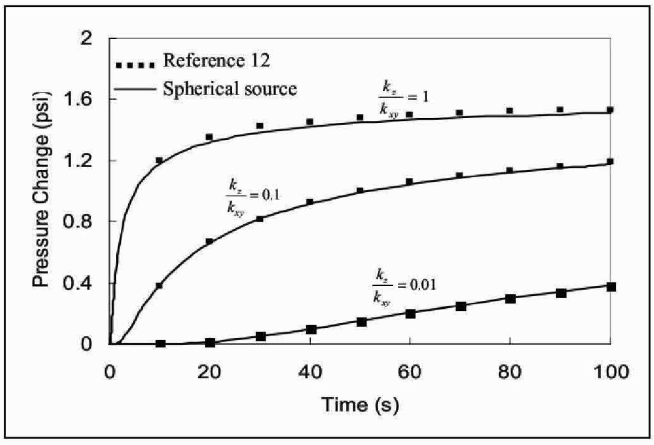

Fig. 12: Pressure response at observation probe based on spherical source model and data in Table 4 compared to Ref. 12

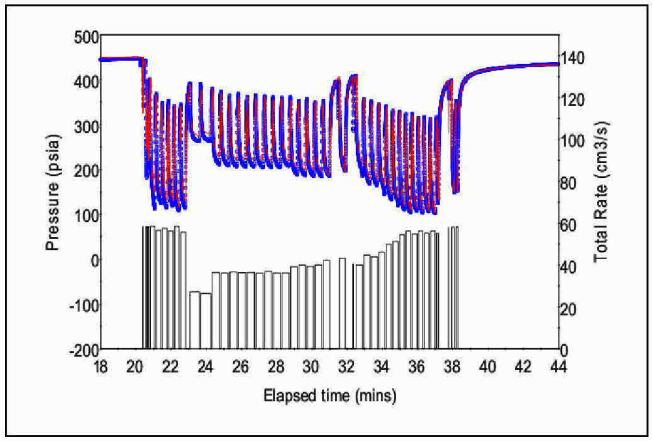

Fig. 13: Example 3. Straddle packer pumping test

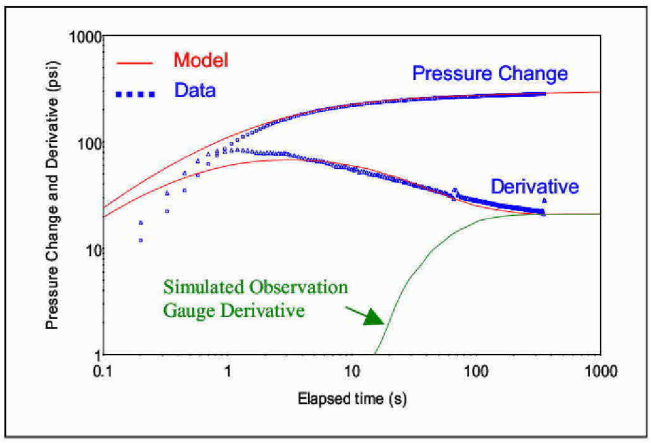

Fig. 14: Example 3. Log-log plot of match of model to build-up data including simulated observation gauge response

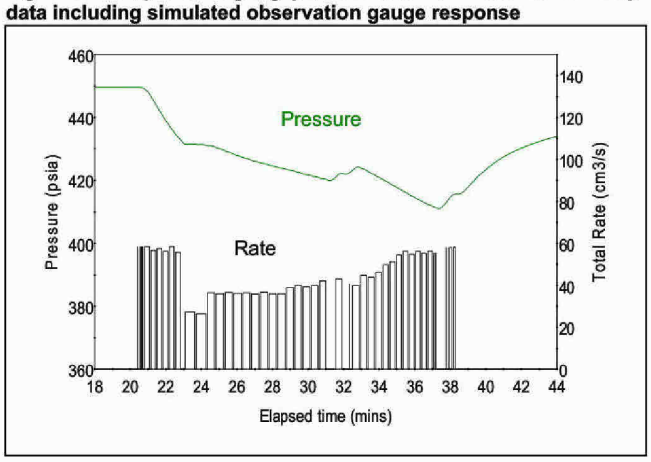

Fig. 15: Example 3. Simulated pressure response of an observation gauge

Parameter	Units	Value
Input Data		
Probe radius, r_p	cm	1.27
Porosity	fraction	0.15
Total compressibility, c_t	1/psi	3E-5
Geometric Factor, G_0		4.67
Match Parameters		
Initial reservoir pressure, p_i	psia	3641
Pressure Match, $\left(p_D\sqrt[3]{C_D}/\Delta p\right)_m$	1/psi	0.0238
Time Match, $\left(t_D/\sqrt[3]{C_D^2}/\Delta t\right)_m$	1/s	1.67
Curve Match, $\left(\sqrt[3]{C_D}\left(1+S_p\right)\right)_m$		3.42
Results		
Spherical mobility, k_{xyz}/μ	mD/cp	1.6
Compressibility, c_{sys}	1/psi	7.3E-6
Skin, S_p		0.32
Useful build-up duration	s	204
Radius of investigation, r_i	cm	120
Formation Rate Analysis		
Initial pressure, p^*_{FRA}	psia	3641
Mobility, k_{FRA}/μ	mD/cp	3.6
Compressibility, c_{sys}	1/psi	7.7E-6

Table 1: Input data and match parameters for Field Example 1

Parameter	Units	Value
Input Data		
Probe radius, r_p	cm	1.27
Porosity	fraction	0.2
Total compressibility, c_t	1/psi	1.5E-5
Geometric Factor, G_0		4.67
Permeability anisotropy, k_z/k_{xy}		1.0
Match Parameters		
Initial reservoir pressure, p_i	psia	3035
Pressure Match, $\left(p_D\sqrt[3]{C_D}/\Delta p\right)_m$	1/psi	0.918
Time Match, $\left(t_D/\sqrt[3]{C_D^2}/\Delta t\right)_m$	1/s	12.89
Curve Match, $\left(\sqrt[3]{C_D}\left(1+S_p\right)\right)_m$		7.21
Curve Match, $\left(d_{topD}\right)_m$		7.66
Curve Match, $\left(d_{botD}\right)_m$		7.66
Results		
Spherical mobility, k_{xyz}/μ	mD/cp	5.82
Compressibility, c_{sys}	1/psi	3.33E-6
Skin, S_p		1.86
Distance to top boundary, d_1	cm	24.5
Distance to bottom boundary, d_2	cm	24.5
Useful build-up duration	s	16
Radius of investigation, r_i	cm	100
Formation Rate Analysis		
Initial pressure, p^*_{FRA}	psia	3033.6
Mobility, k_{FRA}/μ	mD/cp	5.80
Compressibility, c_{sys}	1/psi	4.19E-6

Table 2: Input data and match parameters for Field Example 2

Parameter	Units	Value
Horizontal mobility, k_{xy}/μ	mD/cp	100
Vertical distance, Δz	cm	70
Flow rate, q	cm^3/s	10
Total compressibility, c_t	1/psi	2E-5
Porosity, ϕ	fraction	0.2
Source probe radius, r_p	cm	0.556

Table 3: Data for observation probe response in Fig. 12

Parameter	Units	Value
Input Data		
Straddle Packer Open Interval, h_w	cm	107
Porosity	fraction	0.2
Total compressibility, c_t	1/psi	1.5E-5
Net reservoir thickness, h	cm	457
Wellbore radius, r_w	cm	1.0
Mid point of open interval, z_w	cm	229
Observation probe location, z_p	cm	180
Match Parameters		
Initial reservoir pressure, p_i	psia	
Pressure Match, $\left(p_D/\Delta p\right)_m$	1/psi	0.02384
Time Match, $\left(t_D/C_D/\Delta t\right)_m$	1/s	8.73
Curve Match, $\left(C_D e^{2S}\right)_m$		0.185
Curve Match, $\left(h_D^2/C_D\right)_m$		15325
Results		
Horizontal mobility, k_{xyz}/μ	mD/cp	7.1
Vertical mobility, k_{xyz}/μ	mD/cp	3.5
Skin, S		-0.12
Storage coefficient, C	cm^3/psi	0.159
Useful build-up duration	s	352
Radius of investigation, r_i	cm	500

Table 4: Input data and match parameters for Field Example 3

Symbol	Name	Units				
	Unit System	SI	Darcy	Metric	Oilfield	Customary
a_1	Unit Coefficient	2π	2π	0.053577	0.007082	0.0004275
a_2	Unit Coefficient	1	1	0.0003553	0.0002637	6.8046E-05
a_3	Unit Coefficient	$1/2\pi$	$1/2\pi$	$1/2\pi$	0.8936	$1/2\pi$
B	Formation volume factor	m^3/m^3	cm^3/cm^3	m^3/m^3	bbl/stb	cm^3/cm^3
C'	Shape factor					
C	Storage Coefficient	m^3/Pa	cm^3/atm	m^3/bar	bbl/psi	cm^3/psi
c_g	Gas compressibility	Pa^{-1}	atm^{-1}	bar^{-1}	psi^{-1}	psi^{-1}
c_o	Oil compressibility	Pa^{-1}	atm^{-1}	bar^{-1}	psi^{-1}	psi^{-1}
c_r	Rock compressibility	Pa^{-1}	atm^{-1}	bar^{-1}	psi^{-1}	psi^{-1}
c_{sys}	System compressibility (inside WFT tool)	Pa^{-1}	atm^{-1}	bar^{-1}	psi^{-1}	psi^{-1}
c_t	Total Compressibility	Pa^{-1}	atm^{-1}	bar^{-1}	psi^{-1}	psi^{-1}
c_w	Water compressibility	Pa^{-1}	atm^{-1}	bar^{-1}	psi^{-1}	psi^{-1}
d	Boundary distance	m	cm	m	ft	cm
ϕ	Porosity	fraction	fraction	fraction	fraction	fraction
G_0	Geometric shape factor for FRA					
h	Reservoir Thickness	m	cm	m	ft	cm
h_w	Interval of well open to flow	m	cm	m	ft	cm
k	Permeability	m^2	D	mD	mD	mD
k_d	Drawdown Permeability	m^2	D	mD	mD	mD
k_{FRA}	FRA Permeability	m^2	D	mD	mD	mD
k_{xy}	Horizontal Permeability	m^2	D	mD	mD	mD
k_{xyz}	Spherical Permeability	m^2	D	mD	mD	mD
k_z	Vertical Permeability	m^2	D	mD	mD	mD
μ	Viscosity	Pa.s	cp	cp	cp	cp
p	Pressure	Pa	atm	bar	psi	psi
q	Flow rate	m^3/s	cm^3/s	m^3/day	bbl/day	cm^3/s
r_i	Radius of investigation	m	cm	m	ft	cm
r_p	Probe radius	m	cm	m	ft	cm
r_s	Spherical source radius	m	cm	m	ft	cm
r_w	Wellbore radius	m	cm	m	ft	cm
s	Laplace operator					
S	Skin	-	-	-	-	-
S_g	Gas Saturation	fraction	fraction	fraction	fraction	fraction
S_o	Oil saturation	fraction	fraction	fraction	fraction	fraction
S_w	Water Saturation	fraction	fraction	fraction	fraction	fraction
t	Time	s	s	hrs	hrs	s
Δt	Elapsed Time	s	s	hrs	hrs	s
Δt_{si}	Total shut-in time	s	s	hrs	hrs	s
V_{sys}	System Volume (WFT tool and flowlines)	m^3	cm^3	m^3	bbl	cm^3
z_p	Distance between observation and source probe	m	cm	m	ft	cm
z_w	Height of mid point of open interval above base of reservoir	m	cm	m	ft	cm

Table 5: Nomenclature and Units

Appendix A

Spherical Source with Storage and Skin. Define the following dimensionless parameters:

$$p_D = \frac{a_1 k_{xyz} 2r_s}{q\mu}\Delta p \tag{A-1}$$

$$t_D = \frac{a_2 k_{xyz}}{\phi\mu c_t r_s^2}\Delta t \tag{A-2}$$

$$C_D = \frac{a_3 C}{2\phi c_t r_s^3} \tag{A-3}$$

$$S_p = \frac{a_1 k_{xyz} 2r_s \Delta p_S}{q\mu} \tag{A-4}$$

where:

$$C = V_{sys} c_{sys} \tag{A-5}$$

$$k_{xyz} = \sqrt[3]{k_x k_y k_z} = \sqrt[3]{k_{xy}^2 k_z} \tag{A-6}$$

$$c_t = c_r + S_o c_o + S_g c_g + S_w c_w \tag{A-7}$$

The equation governing pure wellbore storage is

$$p_D = \frac{t_D}{C_D} \tag{A-8}$$

and the late time approximation for pure spherical flow is

$$p_D = 1 - \frac{1}{\sqrt{\pi t_D}} + S_p \tag{A-9}$$

Eq. (A-8) can be rearranged to

$$p_D \sqrt[3]{C_D} = \frac{t_D}{\sqrt[3]{C_D^2}} \tag{A-10}$$

And Eq. (A-9) rearranges to

$$p_D \sqrt[3]{C_D} = \sqrt[3]{C_D}\left(1 + S_p\right) - \frac{1}{\sqrt{\pi \dfrac{t_D}{\sqrt[3]{C_D^2}}}} \tag{A-11}$$

Examination of Eqs. (A-10) and (A-11) illustrates that there are just three independent dimensionless groups that define spherical flow with storage and skin. These are

$$p_D \sqrt[3]{C_D}\ ,\ t_D \Big/ \sqrt[3]{C_D^2} \text{ and } \sqrt[3]{C_D}\left(1 + S_p\right)$$

and define, respectively, the pressure match, time match and curve match when this model is applied to observed data.

Compare these three groups with those used for a fully penetrating vertical well in a uniform thickness infinite acting homogeneous reservoir as identified by Gringarten et al:[18]

p_D, t_D/C_D and $C_D e^{2S}$. with definitions the same as those described in Appendix B.

Of particular importance is the difference in skin factors and their applicable range. For the spherical source, the skin, Sp, must always be greater than -1. Any smaller value would result in zero or negative pressure drops.

Defining the derivative in the usual manner: [19]

$$p'_D = \frac{dp_D}{d\ln t_D} = t_D \frac{dp_D}{dt_D} \tag{A-12}$$

and taking the derivative of Eq. (A-10) yields, for wellbore storage:

$$p'_D \sqrt[3]{C_D} = \frac{t_D}{\sqrt[3]{C_D^2}} \tag{A-13}$$

Both Eqs. (A-10) and (A-13) are represented by the same single unit slope straight line in Fig. 2.

Similarly, the derivative of Eq. (A-11) yields for spherical flow:

$$p'_D \sqrt[3]{C_D} = \frac{1}{2\sqrt{\pi \dfrac{t_D}{\sqrt[3]{C_D^2}}}} \tag{A-14}$$

and is represented by a single negative half unit slope straight line in Fig. 2. The type curve representation of spherical flow and wellbore storage in Fig. 2 is analogous to that for radial flow and wellbore storage described by Bourdet *et al.* [20]

The generation of the complete solution of the model between the two flow regimes requires storage, C_D, and skin, S, to be added to the exact spherical source solution. This is readily done in Laplace space[21]:

$$\bar{p}(C_D, S, s) = \frac{1}{s\left(sC_D + \dfrac{1}{s\bar{p}(s) + S}\right)} \tag{A-15}$$

where $\bar{p}(s)$ is the Laplace transform of the spherical source solution (without storage and skin), and $\bar{p}(C_D, S, s)$ is the resulting Laplace space solution with storage and skin. Laplace inversion can be made using, for example, the Stehfest algorithm.[22]

Upper and lower boundaries can be introduced using the method of images or similar techniques[23] and requires the introduction of permeability anisotropy. The dimensionless distances from the probe to the boundaries become two additional match parameters and are defined:

$$d_{botD} = \frac{d_{bot}}{r_s\left(\dfrac{k_z}{k_{xy}} C_D\right)^{1/3}} \tag{A-16}$$

$$d_{topD} = \frac{d_{top}}{r_s\left(\frac{k_z}{k_{xy}} C_D\right)^{1/3}} \quad \text{(A-17)}$$

If both boundaries are of type no-flow, then radial flow develops and is characterized by stabilization in the derivative which, in Fig. 2, is defined:

$$p'_D \sqrt[3]{C_D} = \frac{1}{d_{topD} + d_{botD}} \quad \text{(A-18)}$$

The observation probe measures the pressure response at a distance, Δz_p, away from the spherical source. Using the same independent dimensionless groups as for the source probe, the dimensionless distance to the observation probe is written:

$$\Delta z_{pD} = \frac{\Delta z_p}{r_s\left(\frac{k_z}{k_{xy}} C_D\right)^{1/3}} \quad \text{(A-19)}$$

Appendix B

Partially Completed Well with Storage and Skin. The following independent dimensionless groups characterize the model:

$$p_D = \frac{a_1 k_{xy} h}{q\mu} \Delta p \quad \text{(B-1)}$$

$$\frac{t_D}{C_D} = \frac{a_2 k_{xy} h}{a_3 \mu C} \Delta t \quad \text{(B-2)}$$

$$C_D e^{2S} = \frac{a_3 C}{\phi c_t h r_w^2} e^{2S} \quad \text{(B-3)}$$

$$h_{wD} = \frac{h_w}{h} \quad \text{(B-4)}$$

$$\frac{h_D^2}{C_D} = \frac{\phi c_t h^3}{a_3 C} \frac{k_{xy}}{k_z} \quad \text{(B-5)}$$

$$z_{wD} = \frac{z_w}{h} \quad \text{(B-6)}$$

If an observation probe exists, the dimensionless distance between the mid point of the open interval and the observation gauge is defined:

$$\Delta z_{pD} = \frac{\Delta z_p}{r_w\left(\frac{k_z}{k_{xy}} C_D\right)^{1/2}} \quad \text{(B-7)}$$